Published OnlineFirst January 22, 2015; DOI: 10.1158/1535-7163.MCT-14-1093-T

Small Molecule Therapeutics

Molecular Cancer Therapeutics

ATF4 Gene Network Mediates Cellular Response to the Anticancer PAD Inhibitor YW3-56 in Triple-Negative Breast Cancer Cells

Shu Wang[1], Xiangyun Amy Chen[1], Jing Hu[1], Jian-kang Jiang[2], Yunfei Li[1], Ka Yim Chan-Salis[1], Ying Gu[1], Gong Chen[3], Craig Thomas[2], B. Franklin Pugh[1], and Yanming Wang[1]

Abstract

We previously reported that a pan-PAD inhibitor, YW3-56, activates p53 target genes to inhibit cancer growth. However, the p53-independent anticancer activity and molecular mechanisms of YW3-56 remain largely elusive. Here, gene expression analyses found that ATF4 target genes involved in endoplasmic reticulum (ER) stress response were activated by YW3-56. Depletion of ATF4 greatly attenuated YW3-56–mediated activation of the mTORC1 regulatory genes SESN2 and DDIT4. Using the ChIP-exo method, high-resolution genomic binding sites of ATF4 and CEBPB responsive to YW3-56 treatment were generated. In human breast cancer cells, YW3-56–mediated cell death features mitochondria depletion and autophagy perturbation. Moreover, YW3-56 treatment effectively inhibits the growth of triple-negative breast cancer xenograft tumors in nude mice. Taken together, we unveiled the anticancer mechanisms and therapeutic potentials of the pan-PAD inhibitor YW3-56. *Mol Cancer Ther; 14(4); 877–88. ©2015 AACR.*

Introduction

Chromatin is composed of DNA and histone proteins and plays an essential role in transcriptional regulation in eukaryotic cells. Covalent modifications of DNA and histone proteins carry additional information beyond the genetic code, which is often referred as epigenetic information that impinges on gene expression to ensure normal development and cell cycle progression. Because of genetic alterations and/or aberrant expression of chromatin enzymes and regulators, deregulation of DNA and histone modifications can result in disease manifestations including cancer and neurodegenerative diseases (1–3). As such, the development of small molecules targeting chromatin factors has been pursued to restore normal gene expression patterns and to induce genes in favor of cell-cycle arrest and cell death for cancer treatment (4–7).

The peptidylarginine deiminase (PAD) family has 5 members, including PAD1, 2, 3, 4, and 6, in the human and mouse genomes (8, 9). PAD4 converts histone Arg and methyl-Arg residues to citrulline via deimination and demethylimination, respectively (10, 11). PAD4 catalyzed histone citrullination represses p53 target gene expression (e.g., p21, PUMA, and SESN2) in coordination with histone deacetylation (6, 12–14). PAD4 is also found to be a target gene of p53 and may form a negative feedback loop to regulate p53 biologic functions, such as apoptosis (15). Besides its role in gene repression, PAD4 citrullinates histone H3 Arg8 residue, thereby counteracting the function of the adjacent histone H3 Lys9 methylation and decreasing heterochromatin protein 1 binding to this methylation site (16, 17) thereby offering a mechanism underlying the proposed gene activation function of PAD4 in serving as a coactivator of Elk-1 (14).

Within the solid tumor microenvironment *in vivo*, cancer cells are under high levels of stresses, including metabolic stress due to the fluctuation of blood and nutrient supply, oxidative stress because of reactive oxygen species (ROS) elevation, and endoplasmic reticulum (ER) stress due to unfolded protein accumulation or a large amount of protein synthesized in the ER (18–20). The tumor suppressor p53 functions as a major node of cellular signaling network in maintaining homeostasis and guarding the genome (21, 22). Because about 50% of cancer cells lack a wild-type p53 (23), other transcription factors are expected to play an important role in regulating gene expression to cope with these cellular stresses and determine the cell fate. ATF4 (activating transcription factor 4) is well-known for its role in the ER stress response that can be induced as a result of an increase in unfolded proteins and amino acid starvation (19, 24–28). In response to the ER stress, the PERK kinase phosphorylates eIF2α, which in turn increases the translation of ATF4 (29, 30). ATF4 regulates the transcription of a cohort of downstream target genes involved in cell survival, apoptosis, autophagy, and senescence (31–34). The ultimate outcome after ATF4 activation is context-dependent, influenced by the nature of the stimulation and the cell type. In this study, we found that YW3-56 induces ER stress, thereby eliciting a robust ATF4 response.

Macroautophagy (hereafter called autophagy) is an evolutionarily conserved cellular process during which a large amount of

[1]Center for Eukaryotic Gene Regulation, Department of Biochemistry and Molecular Biology, Pennsylvania State University, State College, Pennsylvania. [2]National Center for Advancing Translational Sciences, National Institutes of Health, Bethesda, Maryland. [3]Department of Chemistry, Pennsylvania State University, State College, Pennsylvania.

Note: Supplementary data for this article are available at Molecular Cancer Therapeutics Online (http://mct.aacrjournals.org/).

Current address For Y. Li: Thermo Scientific, Life Technologies, Ion Torrent, South San Francisco, California, 94080, USA.

Corresponding Author: Yanming Wang, 454 North Frear Building, Department of Biochemistry and Molecular Biology, Pennsylvania State University, State College, PA 16802. Phone: 814-865-3775; Fax: 814-865-7770; E-mail: yuw12@psu.edu

doi: 10.1158/1535-7163.MCT-14-1093-T

Published OnlineFirst January 22, 2015; DOI: 10.1158/1535-7163.MCT-14-1093-T

cellular components is degraded in sequentially formed phagophores, autophagosomes, and autolysosomes (35–37). Autophagy is triggered as a result of starvation in many organisms and appears to be a cellular process adapted by cancer cells to cope with various stresses, such as starvation and ER stress (19, 38–40). Elevated autophagy facilitates cancer cell to cope with metabolic and therapeutic stresses, thus autophagy perturbation offers new opportunities for medicinal intervention in cancer treatment (6, 19, 41, 42).

We recently reported that a newly developed PAD inhibitor YW3-56 activates p53 target genes and inhibits cancer growth (6). However, it is unknown whether YW3-56 is effective in p53-mutant cancer cells. In this study, we found that YW3-56 activates ATF4 target genes that in turn regulate the mTORC1 signaling pathway. Gene expression microarray and ChIP-exo assays were performed to profile the ATF4 gene network and its biologic functions. We show that YW3-56 inhibits cancer cells growth via the ER stress pathway in breast cancer MDA-MB-231 cells. Moreover, YW3-56 is effective in growth inhibition of tumors derived from the triple-negative breast cancer cells in nude mice, suggesting a therapeutic potential of this inhibitor.

Materials and Methods

Cell culture, reagents, and treatment

MDA-MB-231 and its bone metastasis 1833TR cell lines were obtained from Dr. Massagué (MSKCC, New York, NY) in 2011. Authentication of MDA-MB-231 and 1883TR cells was performed in 2014 using the Promega/ATCC short tandem repeat (STR) DNA fingerprinting, and the cell identity was confirmed. MDA-MB-231 and its derivative 1833TR cells were cultured in DMEM (Gibco) supplemented with 10% FBS and 1% penicillin/streptomycin in a 5% CO_2 incubator at 37°C. Compounds were added when cells reached around 70% confluence for additional analyses. Concentrations and duration of YW3-56 treatment were performed as specified in this article. Other cell lines in Supplementary Fig. S1 were used for the IC_{50} analyses only, including MCF-7, HCC38, HL-60, Jurkat, GDM1, K562, Hel, Caco-2, HT-29, U2OS, HepG2, A549, H1299, S180, and MCF-10A cells, and were obtained from ATCC within the last 5 years and used at early passages stored within 6 month after the receipt of the original stock. HCT116 $p53^{+/+}$ and $p53^{-/-}$ were a generous gift from Dr. Bert Vogelstein at Johns Hopkins University (Baltimore, MD) and obtained in 2008 and stored at early passages. Mouse embryonic fibroblasts cells were established in house using 12- to 13-day-old embryos from C57BL/6 mice. Mouse embryonic stem J1 cells were a generous gift from Dr. Na Xiong at Pennsylvania State University (State College, PA) in 2009 and were previously described (43). HL-60 cells were cultured in RPMI-1640 medium supplemented with 10% FBS and 1% penicillin/streptomycin. DMSO (1.25%) was used to differentiate HL-60 cells into granulocytic lineages for 3 days. For inducing histone H3 citrullination in HL-60 granulocytes, 2×10^6/mL cells were resuspended in Locke solution and treated with 4 μmol/L calcium ionophore A23187 (Sigma) for 25 minutes at 37°C.

Antibodies used in Western blotting were anti-PAD4 (custom-made), anti-His-tag (Abcam, G020), anti-H3Cit (Abcam, ab5103), anti-H3 (Abcam, ab1791), anti-ATF4 (Santa Cruz, sc-200), anti-CEBPB (Bethyl, A302-738A), anti-Nrf2 (Santa Cruz, sc-13032), anti- SESN2 (Abcam, ab57810), anti-DDIT4 (Proteintech Group, 10638-1-AP), anti-DDIT3 (Santa Cruz, sc7351), anti-p70S6K (Cell Signaling, 9202), anti-p70S6K-pT389 (Cell Signaling, 9205), anti-4E-BP1-pS65 (Cell Signaling, 9456), anti-4E-BP1 (Cell Signaling, 9644), anti-LC3B (Cell Signaling, 2775), anti-p62/SQSTM1 (Bethyl Laboratories, A302-855A), anti-cleaved-PARP (Asp214; Cell signaling, 9546), anti-eIF2α (Cell Signaling, 2103), anti-eIF2α-pS51 (Cell Signaling, 3398), and anti-β-actin (Sigma, A1978) at appropriate dilutions.

ChIP-exo

ChIP-exo assays were carried out essentially as described with minor alterations (44). Immunoprecipitated DNA fragments for ChIP-exo were prepared from MDA-MB-231 cells treated with 12 μmol/L YW3-56 or vehicle for 6 hours and then subjected to 1% formaldehyde crosslinking for 10 minutes. After being quenched with 125 mmol/L final concentration of glycine for 5 minutes, cells were harvested and washed. Sonicated chromatin was prepared by standard methods. Chromatin immunoprecipitation (ChIP) was performed with anti-ATF4 (Santa Cruz, sc-200) and anti-CEBPB (Bethyl, A302-738A) using standard ChIP methods. Lambda exonuclease treatment and library construction were performed as previously described (45). In total, 5 replicates from 3 biologic experiment sets were done for each antibody following the same protocol. Sequencing was performed using Illumina HiSeq 2000 at Penn State University. Reads generated by ChIP-exo experiment were aligned to the UCSC human genome hg19 (http://genome.ucsc.edu) using BWA with default parameters (46). Uniquely aligned tags were retained and filtered to remove those from blacklist regions provided by the ENCODE project. The resulting distribution of reads was used to identify the forward (W)- and reverse (C)-strand peaks using GeneTrack with sigma = 5 and exclusion zone = 10 (47, 48). The W and C peaks were paired if they were 3′ to each other and less than 60 bp apart. Because the analysis of individual replicates displays significant consistence in predicted target genes, tags from 5 replicates were merged together for final peak-pair calls. According to the normal distribution of tag counts of peak-pairs in IgG data set, we assumed that 99% of the peak-pairs, which have a tag count of less than 9 (mean + 3 SD), is background noise. Correspondingly, peak-pairs that have a tag count of less than 9 were first removed from merged data sets of IgG, ATF4, and CEBPB. Tag counts of peak-pairs retained in each data set were still normally distributed. For reliability, less than top 1% peak-pairs—top 1,500 peak-pairs that have a tag count more than 26 from the ATF4 dataset and top 1,500 peak-pairs that have a tag count more than 27 from the CEBPB data set—were used for predicting target genes. A total of 35 peak-pairs met the criteria of tag count more than 26 from the IgG dataset were used to generate a list of unspecific antibody recognition sites.

Identification of ATF4 and CEBPB target genes and binding motifs

Binding sites identified by ChIP-exo of ATF4 (1,500 peak-pairs), CBEPB (1,500 peak-pairs), and IgG (35 peak-pairs) were assigned to the nearest RefSeq TSSs within 25 kb on either strands using the UCSC human genome hg19 annotation, yielding 589, 610, and 13 genes, respectively. By filtering away the potential unspecific targets of antibody, 579 and 607 target genes were identified for ATF4 and CEBPB, respectively. Each binding site would only be assigned to one transcription start site (TSS), whereas one TSS might be associated with multiple binding sites. Motif analyses of the top 1,500 binding locations were performed using the MEME suite

(http://meme.nbcr.net/meme/; ref. 49). Sequences fetched from the top 1,500 binding locations (sequence −50 bp to +50 bp from the peak pair midpoint) were subjected to MEME-ChIP (50). The top-scoring motif for each factor was identified as the consensus motif 1. The sequences without the motif 1 may represent a different mode of factor binding and were not further analyzed. Motif 1 discovered by MEME was then subjected to the FIMO analyses to find individual motif occurrences using default parameters (51). Motif 1 containing sequences (914 sites for ATF4 and 1,277 sites for CEBPB) were reported by FIMO.

Functional enrichment analyses

Functional enrichment analyses on 579 ATF4 and 607 CEBPB putative target genes identified by ChIP-exo were performed using the DAVID tools (52) to identify significantly overrepresented biologic functions defined by Gene Ontology terms. Enrichment score is used to rank the biologic significance of the gene groups.

qRT-PCR and Western blot analyses

Cells harvested from 6-well plates were washed with PBS, and total RNA was extracted using the RNeasy Mini Kit (Qiagen) following the manufacturer's instructions. Quantitative reverse transcription PCR (qRT-PCR) was done using qScript cDNA SuperMix (Quanta Biosciences) as previously described (6). Quantitative PCR of specific genes was performed using SYBR Green SuperMix (Quanta Biosciences) in the StepOnePlus Real-Time PCR System (Applied Biosystems). Primers used in quantitative PCR are listed in Supplementary Table S1. Western blot analyses were performed essentially as described previously (6). Antibodies used in Western blotting were listed in Supplementary Materials and Methods.

Microarray, IPA analyses, and GSEA analyses of global gene expression changes

MDA-MB-231 cells were treated with 8 μmol/L YW3-56 for 8 hours before harvesting. Control cells were mock treated with DMSO. Total RNA was extracted as described above. The Affymetrix GeneChip Human Gene 1.0 ST arrays were used. Data from all Affymetrix GeneChips were normalized and analyzed as previously described (6). In total, 1,204 genes with a minimum of 1.5-fold difference and an FDR < 0.05 ($n = 3$) were analyzed using IPA (Ingenuity System, www.ingenuity.com) core analysis to identify canonical pathways, upstream regulators, and establish networks. Top canonical pathways were identified, including the oxidative stress response ($P = 1.86 \times 10^{-5}$), the GADD45 signaling ($P = 9.05 \times 10^{-4}$), and the ER stress pathway ($P = 4.65 \times 10^{-3}$). Moreover, upstream regulators were identified, including ATF4 and EIF2AK3. Target molecules of ATF4 in dataset and their expression changes were graphed. Network analyses visualized the *ATF4-DDIT4* and *SESN2-AMPK-mTORC1* gene networks based on the correlation of genes. Gene set enrichment analyses (GSEA) were performed using microarray data processed by the AltAnalyze software (Gladstone Institution, UCSF; ref. 53) with $P < 0.05$ and 1.5-fold difference as cutoff values. The enrichment of genes in different biologic processes and pathways was evaluated using GSEA with c2 curated gene sets and c5 curated GO gene sets in the MSigDB (54). Enrichment of gene sets was ranked according to normalized enrichment score (NES). The microarray data were submitted following the MIAME guidelines. The GEO accession number for the microarray data is GSE46590.

siRNA treatment and forced overexpression of ATF4 and CEBPB

With a 70% to 80% confluence in 6-well plates, MDA-MB-231 cells were transfected using the siRNA transfection reagent (Santa Cruz) per manufacturer's instructions. siRNAs used in the transient transfections were control scrambled siRNA (Santa Cruz, sc-37007), CEBPB siRNA (Santa Cruz, sc-44251), ATF4 siRNA (Santa Cruz, sc-35112), and PERK siRNA (Santa Cruz, sc-36213). Following siRNA treatment for 48 hours, cells were treated with YW3-56. To analyze the effects of siRNA treatment on YW3-56–mediated cell killing, control scrambled siRNA, ATF4 siRNA, SESN2 siRNA (Santa Cruz, sc-106544), and DDIT4 siRNA (Santa Cruz, sc-45806) were transfected into 1833 cells. At 24 hours following transfection, YW3-56 was added to treat the cells and cell growth was analyzed 48 hours later. To overexpress ATF4 or CEBPB, with a 70% to 80% confluence in 6-well plate, MDA-MB-231 cells were transfected with pRK-ATF4 (Addgene, 26114) plasmid or pCMV-CEBPB (Origene, sc319561) plasmid. Empty pRK and pIRES plasmids were used as negative control. At 24 hours after forced expression of ATF4 and CEBPB, qRT-PCR and Western blotting were performed to analyze the effects of ATF4 and CEBPB on gene expression.

Fluorescent and TEM microscopy

To visualize the LC3B subcellular localization, MDA-231 cells were treated with 8 μmol/L YW3-56 for 12 hours and fixed in 3.7% paraformaldehyde in PBS buffer containing 0.1% Triton X-100 and 0.2% NP-40, pH 7.4. Primary antibody LC3B (Cell signaling) was 1:200 diluted in PBST supplemented with 2% BSA and 5% normal goat serum. Cells were stained with the L3CB antibody overnight at 4°C and then washed with PBST for 3 × 10 minutes and stained with Alex488-conjugated secondary antibody at room temperature for 2 hours in the dark as previously described (11). Nuclear DNA was visualized by Hoechst staining. Imaging was obtained using an Axioskop 40 fluorescence microscope (Carl Zeiss, Inc.) equipped with an AxioCam MRM camera and the AxioVision AC software. For transmission electronic microscopy (TEM) analyses, MDA-MB-231 cells were treated with 10 μmol/L YW3-56 for 8 hours and fixed in 2% glutaraldehyde in 0.1 mol/L phosphate buffer, pH 7.4. TEM imaging was performed in the Penn State Electron Microscopy Facility.

Live cell imaging of mCherry-GFP-LC3

MDA-MB-231 cells were transfected with the mCherry-GFP-LC3B reporter plasmid. The transfection was performed using Lipofectamine 2000 (Invitrogen) in a 35-mm glass bottom dish according to the manufacturer's instructions. Cells were cultured for 12 hours after transfection, before the addition of YW3-56. After incubation with YW3-56 for 12 hours, the live cell imaging was done essentially as previously described (6). The processing and analysis of images were done using Metamorph (Molecular Devices) and the NIH ImageJ software.

MDA-MB-231 cell xenograft analyses in nude mice, hematoxylin and eosin staining

All animal procedures were approved by the Penn State University IACUC committee. To establish the subcutaneous breast cancer xenograft, 1833TR cells were trypsinized, washed, and resuspended in PBS (Gibco) at 5×10^7 cells/mL. Fifty microliters containing 2.5×10^6 cells was injected subcutaneously at both sides of the abdominal mammary fat pad of 5 week-old nude mice

Published OnlineFirst January 22, 2015; DOI: 10.1158/1535-7163.MCT-14-1093-T

(Harlan Lab). After tumors achieved approximately 30 to 50 mm^3, tumor-bearing mice were randomly grouped into 3 mice per group and injected with YW3-56 (12.5 mg/kg daily for 29 days, 25 mg/kg daily for 32 days, or 40 mg/kg once every 2 days for 26 days) or vehicle (10% DMSO in PBS). Tumor volume and body weight were measured daily to evaluate the antitumor activity of YW3-56. At the end point of the experiments, mice were sacrificed. Tumors and important organs (brain, lung, heart, liver, spleen, and kidney) were dissected and weighed. A section of the tumors were used for RNA and protein extraction. Tumor tissues were fixed in formalin, and hematoxylin and eosin (H&E) staining were performed using the service of the ADL (animal diagnostic laboratory) at Penn State University.

Statistics

Data for descriptive statistics analyses are presented as mean values with error bars indicating ± SD or ± SEM. Experiments are repeated, and the numbers of the biologic replicates (n) used for data analyses are indicated in the figures. The Student t test (unpaired, 2-tailed) was used to compare 2 groups of independent samples. Western blotting results are representative results from 2 or 3 independent experiments.

Results

Pan-PAD inhibitor YW3-56 inhibits histone citrullination and cell growth of p53-mutant cancer cells

YW3-56 is a structural mimic of the PAD4 substrate peptidylarginine (Supplementary Fig. S2A), and inhibits PAD4-mediated histone citrullination via covalent modification of PAD4 (Supplementary Fig. S2B–S2D). We analyzed the killing efficacy (IC50) of YW3-56 on a panel of cancer cell lines of different tissue origins and p53 status and found that YW3-56 demonstrated an IC_{50} below 10 μmol/L in breast cancer, leukemia, and colorectal cancer cell lines largely independent of the p53 status while low cytotoxicity to normal cells (Supplementary Fig. S1A).

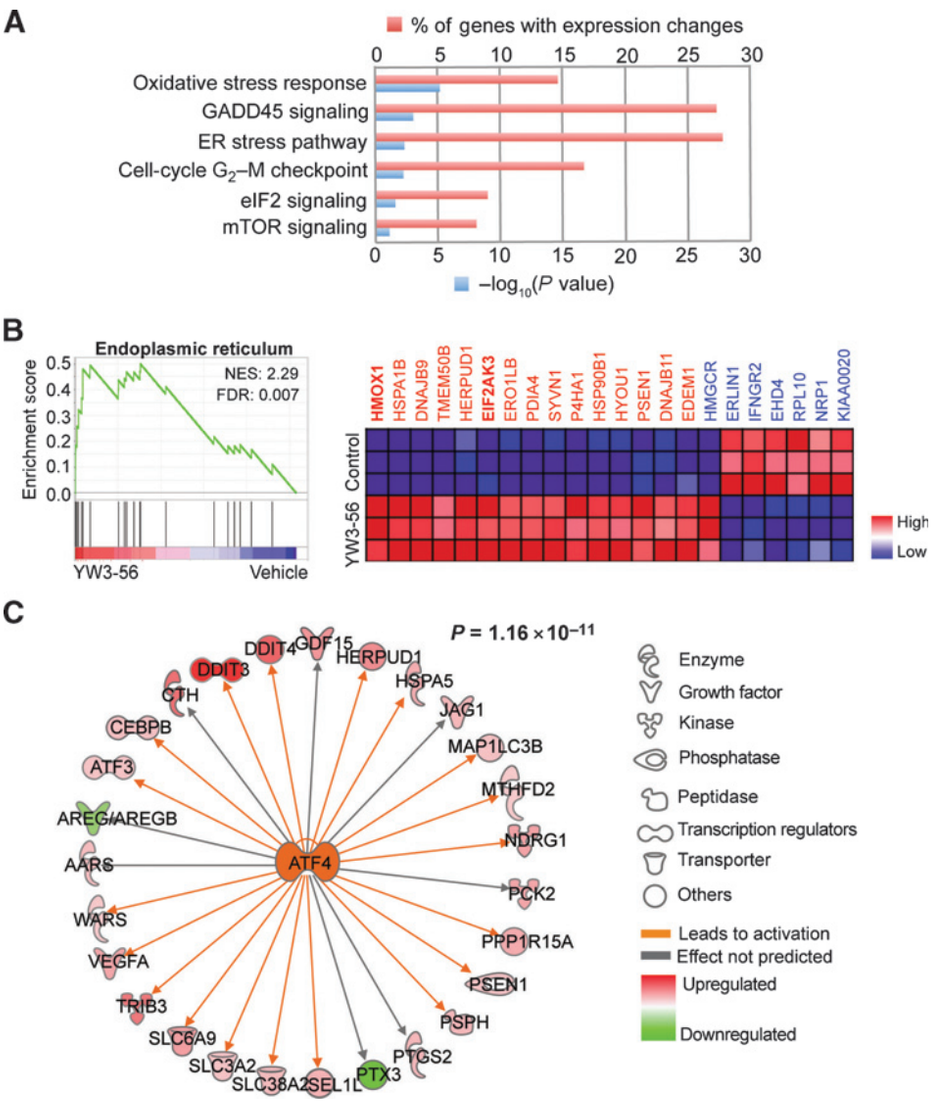

Figure 1.
ER stress response genes are prominently affected in YW3-56–treated MDA-MB-231 cells. A, the IPA analyses of microarray data found canonical pathways significantly affected by YW3-56 treatment. B, GSEA assays found that gene sets important for ER protein homeostasis are enriched after YW3-56 treatment. The normalized enrichment scores (NES) and FDR are shown. Color index represents gene expression changes, and the leading edge genes are colored red. C, the expression of ATF4 target genes was significantly ($P = 1.16 \times 10^{-11}$) altered after YW3-56 treatment.

Published OnlineFirst January 22, 2015; DOI: 10.1158/1535-7163.MCT-14-1093-T

ER stress response genes are prominently activated in MDA-MB-231 cells after YW3-56 treatment

Triple-negative breast cancers lack estrogen receptor (ER), progesterone receptor (PR), and amplified Her2 for targeted therapy and have a great need for novel drug target development. YW3-56 inhibited the growth of the triple-negative breast cancer MDA-MB-231 (carrying the p53R280K mutation) and its derivative 1833 cells after bone metastasis (55). In contrast, the nontumorigenic MCF10A breast epithelial cells were not efficiently killed by YW3-56 (Supplementary Fig. S1B), indicating a therapeutic window for this compound. To analyze the molecular mechanisms, we performed gene expression microarray analyses. In total, 1,204 genes with $\geq$1.5-fold increase or decrease in expression were identified ($P < 0.01$, $n = 3$; Supplementary Table S2). Using 2 independent microarray data analysis tools (IPA and GSEA), we found that the ER stress/unfolded protein response (UPR) genes are significantly altered after YW3-56 treatment (Fig. 1A and B).

ATF4 is a key upstream transcription factor mediating YW3-56 response

To identify transcription factor(s) regulating YW3-56 responses, we used the upstream regulator analyses tool in IPA and identified ATF4 as a high confidence ($P = 1.16 \times 10^{-11}$) regulator of cellular response to YW3-56 (Fig. 1C). ATF4 target genes, such as *DDIT4*, *SESN2*, *CEBPB*, and *DDIT3*, were strongly induced by YW3-56 (Supplementary Table S2). Moreover, IPA

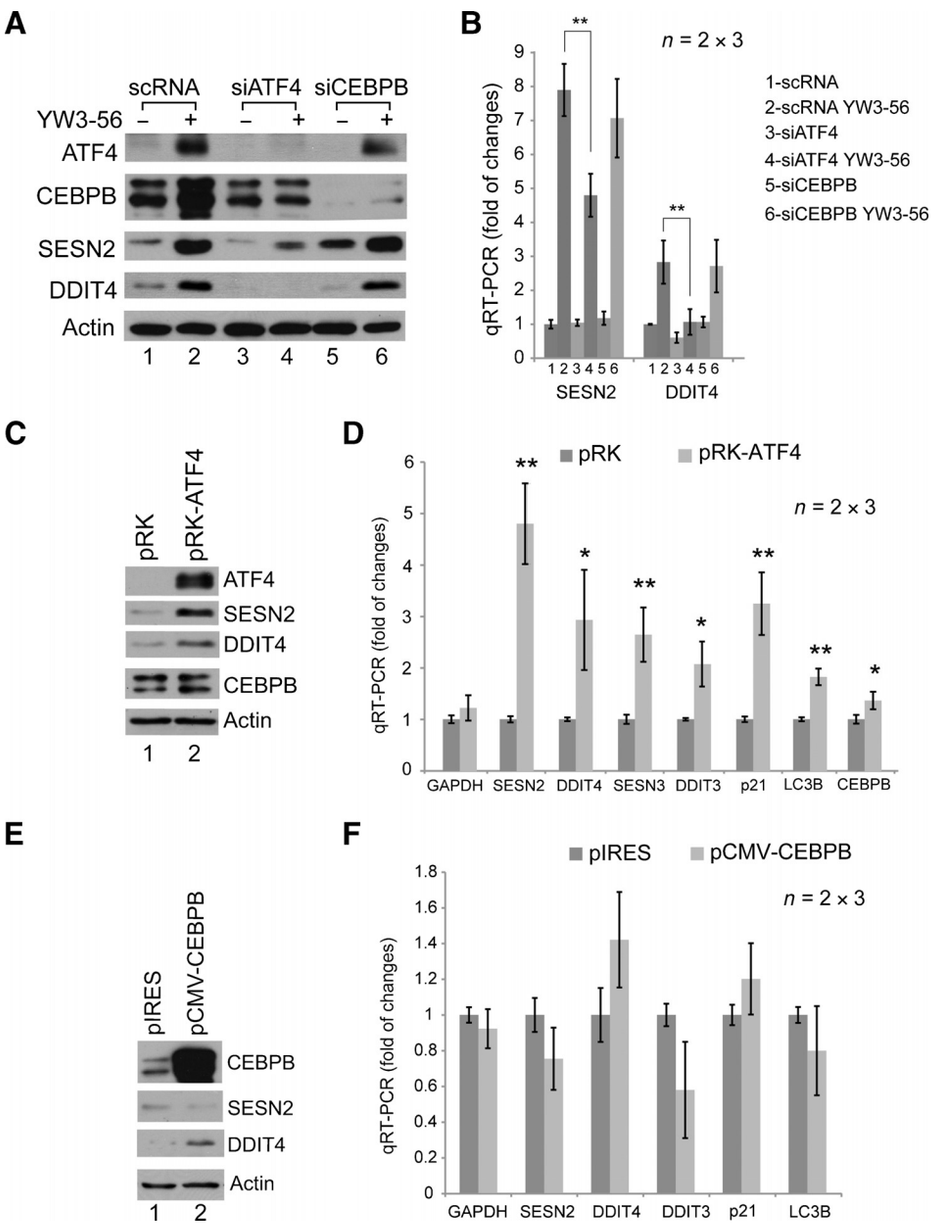

Figure 2.
ATF4 but not CEBPB is essential for SESN2 and DDIT4 induction by YW3-56 in MDA-MB-231 cells. A and B, Western blotting and qRT-PCR analyses of SESN2 and DDIT4 induction after YW3-56 treatment in MDA-MB-231 cells with control, ATF4, and CEBPB siRNA treatment. **, $P < 0.002$; $n = 2 \times 3$. C and D, effects of forced ATF4 expression on SESN2 and DDIT4 protein and mRNA levels. *, $P < 0.01$; **, $P < 0.002$; $n = 2 \times 3$. E and F, effects of forced CEBPB expression on SESN2 and DDIT4 protein and mRNA levels. $n = 2 \times 3$.

Published OnlineFirst January 22, 2015; DOI: 10.1158/1535-7163.MCT-14-1093-T

gene network analyses found that the ATF4-DDIT4-TRIB3 ($P = 1.0 \times 10^{-31}$) and the SESN2-AMPK-TORC1 ($P = 1.0 \times 10^{-24}$) gene networks have significant changes after YW3-56 treatment (Supplementary Fig. S3A and S3B; refs. 56, 57).

ATF4 is a bZIP transcription factor, which can form homodimers or heterodimers with other bZIP proteins (e.g., CEBPB) to regulate transcription (24, 58, 59). Consistent with the idea that YW3-56 triggers the ER stress and activates ATF4 target genes, ATF4 protein and the expression of its target genes (e.g., SESN2 and DDIT4) were increased after YW3-56 treatment (Fig. 2A and B). RNA interference assays found that ATF4 but not CEBPB is required for the basal and induced amount of SESN2 and DDIT4 expression (Fig. 2A and B), suggesting that ATF4 is an important mediator of YW3-56 response in MDA-MB-231 cells. Moreover, after ectopic expression of ATF4 and CEBPB, ATF4 induced the expression of SESN2, DDIT4, and DDIT3 at both protein and mRNA levels (Fig. 2C and D) whereas CEBPB had only subtle effects (Fig. 2E and F). Thus, ATF4 activates UPR genes after YW3-56 treatment, without necessarily involving CEBPB. ChIP analyses detected ATF4 binding at SESN2 and DDIT4 gene promoters after YW3-56 treatment (Supplementary Fig. S4A and S4B), suggesting that ATF4 plays a direct role in the activation of these genes.

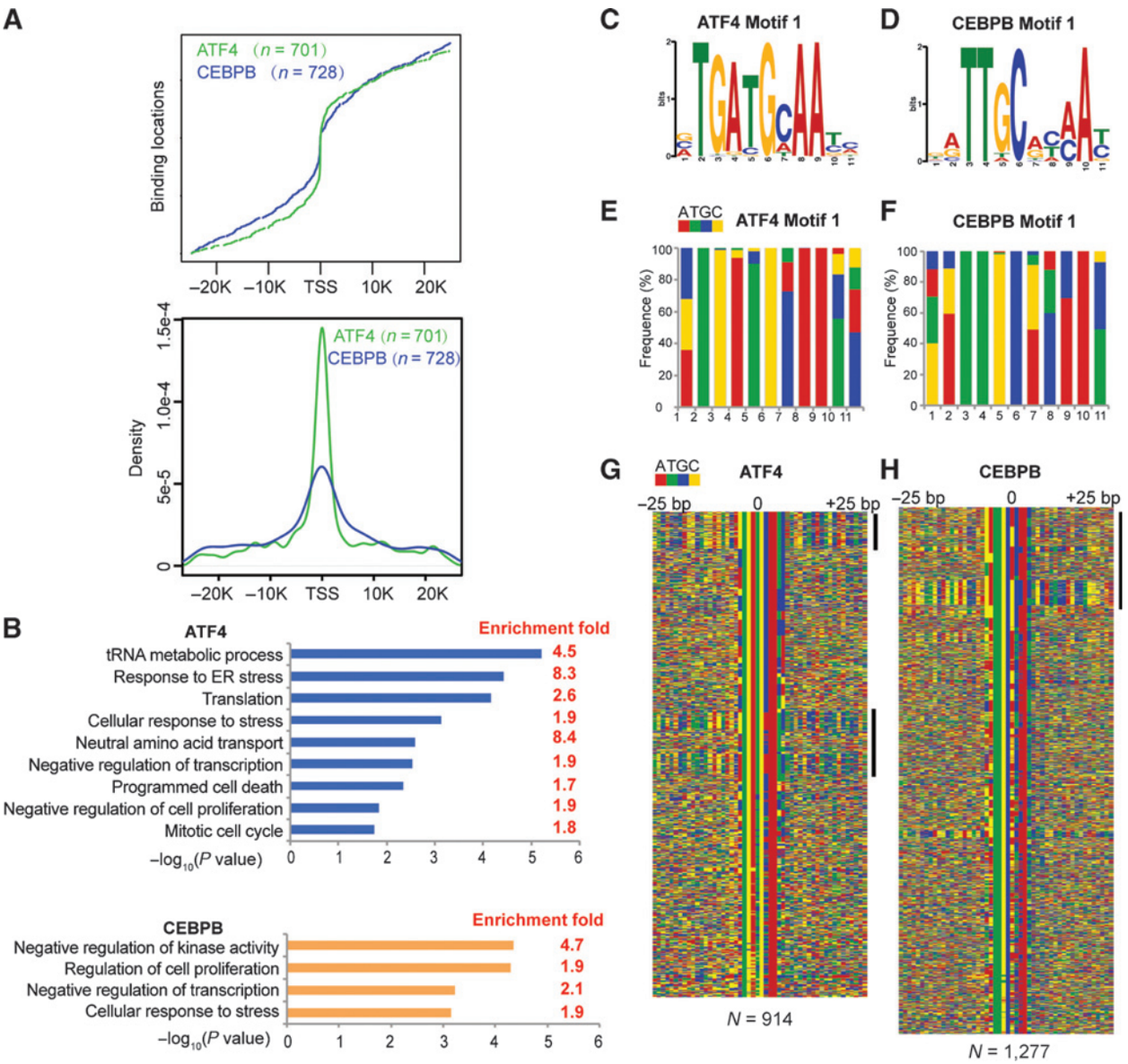

Figure 3.
ChIP-exo identification of ATF4- and CEBPB-binding sites and recognition motifs. A, coordinate plot and density plot of ATF4- and CEBPB-binding locations within the −25 to +25 kb region of target gene promoters. B, function enrichment analysis of ATF4 and CEBPB target genes. C and D, ATF4- and CEBPB-binding motif 1 identified by MEME analyses. E and F, the frequency of ATGC in ATF4 and CEBPB motif 1 was plotted. G and H, FIMO plot analyses of 914 ATF4 motif 1 sites and 1,277 CEBPB motif 1 sites. 50-bp sequences centered on motif 1 were aligned.

Published OnlineFirst January 22, 2015; DOI: 10.1158/1535-7163.MCT-14-1093-T

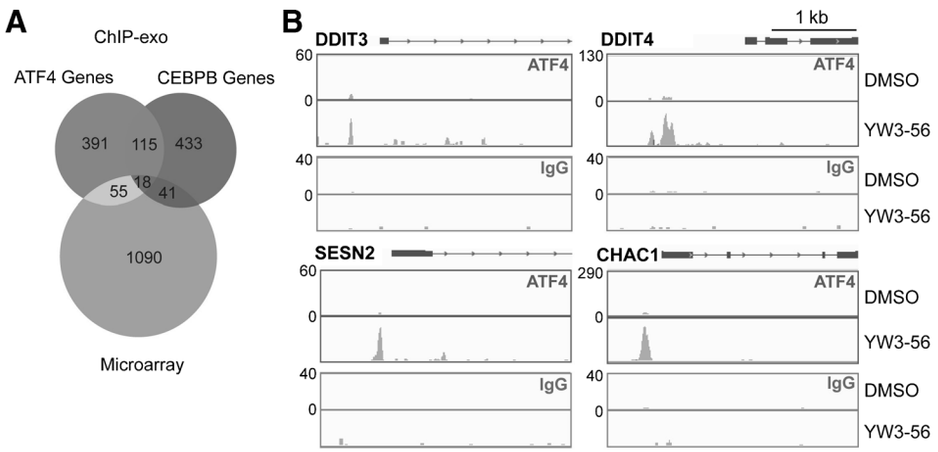

Figure 4.
A subset of ATF4 candidate genes is responsive to YW3-56. A, overlapping of ATF4 and CEBPB candidate genes with genes identified in the microarray assays after YW3-56 treatment. B, screen shots of ATF4 binding on promoters of 4 genes highly responsive to YW3-56.

ChIP-exo identification of genome-wide ATF4-binding sites after YW3-56 treatment

To address how ATF4 regulates transcription in response to YW3-56 treatment, we analyzed the genome-wide binding of ATF4 and CEBPB as a control using the newly developed high-resolution ChIP-exo method (45). Among the top 1,500 binding sites, 701 ATF4 sites and 728 CEBPB sites were mapped to the −25 to +25 kb region of RefSeq genes (based on the h19 human genome annotation; Fig. 3A). Relative enrichment and density mapping plots indicate both ATF4 and CEBPB binding sites are enriched around the TSS (Fig. 3A). The IgG ChIP-exo control samples identified 13 potential nonspecific genes. After removing nonspecific genes, we found that 579 genes have nearby ATF4-binding sites (Supplementary Table S3) and 607 genes have nearby CEBPB-binding sites (Supplementary Table S4). ATF4 candidate genes are enriched in biologic function groups, such as tRNA metabolism and ER stress response, whereas CEBPB candidate genes are involved in kinase activity regulation and cell proliferation (Fig. 3B). Furthermore, ATF4 and CEBPB have overlapping candidate genes involved in cell proliferation and transcriptional regulation.

Next, we performed motif analyses of the top 1,500 ATF4 and CEBPB binding locations using the MEME suite. Of the 1,500 ATF4-binding sites, 914 (∼61%) contain a canonical ATF4 motif [TGATG(C/A)AA] (Fig. 3C), whereas 1,277 of the 1,500 CEBPB-binding sites (∼85%) contain a canonical CEBPB motif [TTGC(A/G)(C/T)(A/C)A] (Fig. 3D). The ATGC frequency in the canonical motifs was shown for ATF4- and CEBPB-binding sites to demonstrate motif reservation (Fig. 3E and F). Sequence alignment of 50-bp DNA sequences centered on the canonical motif (hereafter called motif 1) shows the sequence features of these sites (Fig. 3G and H). Taken together, ChIP-exo provided a precise genome-wide view of ATF4 and CEBPB binding upon ER stress induction by YW3-56.

ATF4 and CEBPB candidate genes responsive to YW3-56 treatment

To analyze the effects of YW3-56 on ATF4 and CEBPB candidate genes, we queried the microarray results. After YW3-56 treatment, 73 ATF4 and 59 CEBPB candidate genes showed significant changes of gene expression (Fig. 4A and Supplementary Table S5). Sequence tag density map showed that after YW3-56 treatment, ATF4 binds much stronger at several highly inducible candidate genes, including DDIT3, DDIT4, SESN2, and CHAC1 (Fig. 4B), as well as CSTF2T, GEMIN7, HSPA9, and WDR36 (Supplementary Fig. S5A). In

Table 1. Functional categories of ATF4-associated genes

Response to unfolded protein	Transcription	Metabolism	Oxidative stress	Others
CHAC1	ARNTL	ADORA2B	SESN2	BBS10 cilia formation
DDIT3	BRF2	AGPAT9	TXNL4B	CSTF2T RNA processing
DNAJB1	CBX4	ALOXE3	TXNRD1	GEMIN7 RNA processing
DNAJB5	CEBPB	DPYSL2		WDR36 RNA processing
HERPUD1	JDP2	GFPT1	DNA damage response	AP3S2 intracellular transport
HSPA5	JHDM1D	GPT2	DDIT4	CLTCL1 intracellular transport
PPP1R15A	KCTD14	MOCS3	GADD45A	CRISPLD2 extracellular matrix
TRIB3	MKX	MTHFD2	TIPIN	FMNL1 cell adhesion
WIPI1	NCOA7	PCK2		MLPH cell motility
XBP1	NFIL3	SLC3A2	Cell signaling	TUFT1 extracellular matrix
	RUNX2	SLC7A11	CDCP1	CCDC9 unknown
	STOX1	VLDLR	EVI2A	FAM102A unknown
	TSC22D3	WARS	GDF15	FAM27C unknown
	ZFP69B	ALDH2	RGMB	RHBDD2 unknown
	ZNF419	ASB1	RND3	TES unknown
	ZNF682		MKNK2	DLGAP1-AS1 ncRNA
				MALAT1 LincRNA
				NBR2 ncRNA
				SNORD83B RNA processing
				SNORD96A unknown

Published OnlineFirst January 22, 2015; DOI: 10.1158/1535-7163.MCT-14-1093-T

contrast, ATF4 binding at EVI2A and RUNX2 does not increase (Supplementary Fig. S5B), suggesting that ATF4 prefers certain targets sites for binding after YW3-56 treatment. These 73 ATF4 associated and YW3-56 inducible genes are involved in diverse biologic functions, such as response to UPR, transcription, and metabolism (Table 1).

YW3-56 induces ER stress and activates ATF4 through the PERK–eIF2α signaling cascade

ATF4 translation is activated by PERK-mediated eIF2α phosphorylation during ER stress response (Fig. 5A; refs. 29, 30). We found that the PERK protein was upshifted [an indicator of PERK phosphorylation and activation (ref. 28)] in YW3-56 concentration–dependent manner at 4 hours after drug treatment (Fig. 5B). Furthermore, the phosphorylation of eIF2α at the PERK target site Ser51 was significantly increased with a concomitant increase of the ATF4 protein (Fig. 5B). Thus, YW3-56 induced UPR and activated the PERK–eIF2α–ATF4 signaling cascade. After PERK depletion with siRNAs, YW3-56 did not induce eIF2α Ser51 phosphorylation and the accumulation of ATF4 (Fig. 5C). Concomitantly, SESN2 induction by YW3-56 was attenuated after PERK depletion (Fig. 5D). Above results suggest that PERK activity

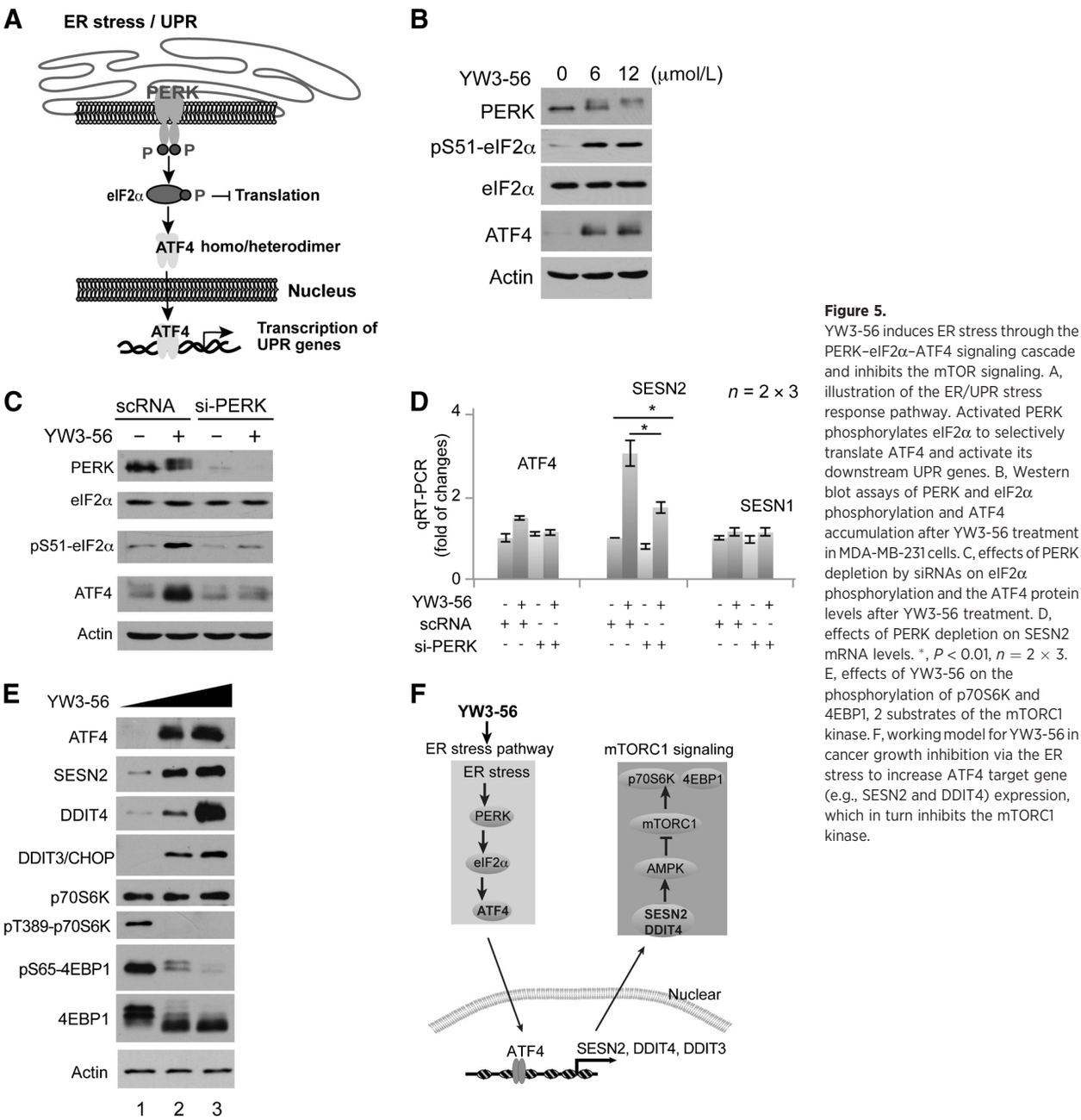

Figure 5.
YW3-56 induces ER stress through the PERK–eIF2α–ATF4 signaling cascade and inhibits the mTOR signaling. A, illustration of the ER/UPR stress response pathway. Activated PERK phosphorylates eIF2α to selectively translate ATF4 and activate its downstream UPR genes. B, Western blot assays of PERK and eIF2α phosphorylation and ATF4 accumulation after YW3-56 treatment in MDA-MB-231 cells. C, effects of PERK depletion by siRNAs on eIF2α phosphorylation and the ATF4 protein levels after YW3-56 treatment. D, effects of PERK depletion on SESN2 mRNA levels. *, $P < 0.01$, $n = 2 \times 3$. E, effects of YW3-56 on the phosphorylation of p70S6K and 4EBP1, 2 substrates of the mTORC1 kinase. F, working model for YW3-56 in cancer growth inhibition via the ER stress to increase ATF4 target gene (e.g., SESN2 and DDIT4) expression, which in turn inhibits the mTORC1 kinase.

Published OnlineFirst January 22, 2015; DOI: 10.1158/1535-7163.MCT-14-1093-T

is important for YW3-56–induced activation of ATF4 and its downstream target genes.

SESN2 and DDIT4 are upstream inhibitors of the mTORC1 kinase. With the SESN2 and DDIT4 induction, YW3-56 treatment decreased the phosphorylation of mTORC1 substrates including p70S6K and 4EBP1 (Fig. 5E). To further test the effects of ER stress on mTORC1, we treated MDA-MB-231 cells with the canonical ER stress inducer thapsigargin. We found that thapsigargin induced the accumulation of ATF4, SESN2, and DDIT4 at protein and mRNA levels (Supplementary Fig. S6A and S6B). A decrease in the phosphorylation of p70S6K and 4EBP1 was detected after thapsigargin treatment (Supplementary Fig. S6A), suggesting that mTORC1 inhibition is a general cellular event following ER stress. Above results favor a model that ATF4 downstream target gene expression in turn leads to the inhibition of mTORC1 upon YW3-56 treatment in MDA-MB-231 cells (Fig. 5F).

To analyze whether ATF4, SESN2, and DDIT4 protein levels impact on YW3-56–mediated cell killing, we depleted these proteins in 1833 cells that are derived from the parental MDA-MB-231 cells after bone metastasis (55). Depletion of ATF4 led to slow growth of 1833 cells (Supplementary Fig. S7A). However, the ATF4 siRNA–transfected cells showed minor but statistically significant less sensitivity to the treatment of YW3-56 at 16 μmol/L for 48 hours (Supplementary Fig. S7B), suggesting that ATF4 plays a partial role in YW3-56–mediated cell killing. Upon activation, ATF4 activates SESN2 and DDIT4, which in turn regulate mTOR. Therefore, we simultaneously depleted SESN2 and DDIT4 in 1833 cells with siRNAs. Cell growth rate was constantly decreased after SESN2/DDIT4 depletion (Supplementary Fig. S7C). In contrast, the SESN2- and DDIT4 siRNA–transfected cells were significantly less sensitive to YW3-56–mediated cell growth inhibition (Supplementary Fig. S7D). Taken together, above results suggest that the ATF4-SESN2/DDIT4 transcription circuit maintains cell viability under normal culture conditions. In contrast, upon induction by ER stress, these proteins facilitate YW3-56–mediated cell killing.

YW3-56–mediated cell death features mitochondria depletion and autophagy perturbation

Treatment of MDA-MB-231 cells with YW3-56 increased the staining of propidium iodide (PI) and Annexin V—2 cell death markers while decreased the staining of MitoTracker Deep Red—a fluorescent dye detecting the mitochondria membrane potential (Supplementary Fig. S8A). Furthermore, the YW3-56–treated cells did not show an increase in PARP cleavage, a canonical apoptosis marker (Supplementary Fig. S8B). Compared with control cells (Fig. 6A), YW3-56–treated cells showed an increase in autophagic vesicles with a concomitant decrease in mitochondria (Fig. 6A). Moreover, immunostaining showed an increased in LC3B vesicles (Fig. 6B). Using the RFP-GFP-LCB reporter to indicate the pH of autophagic vesicles in live cells, an inhibition of autophagosomes to autolysosomes conversion after YW3-56 treatment was detected (Fig. 6C and D). Moreover, the autophagy-mediated degradation of LC3B-II and the p62/SQSTM1 proteins was inhibited after YW3-56 treatment (Fig. 6E). Taken together, these results

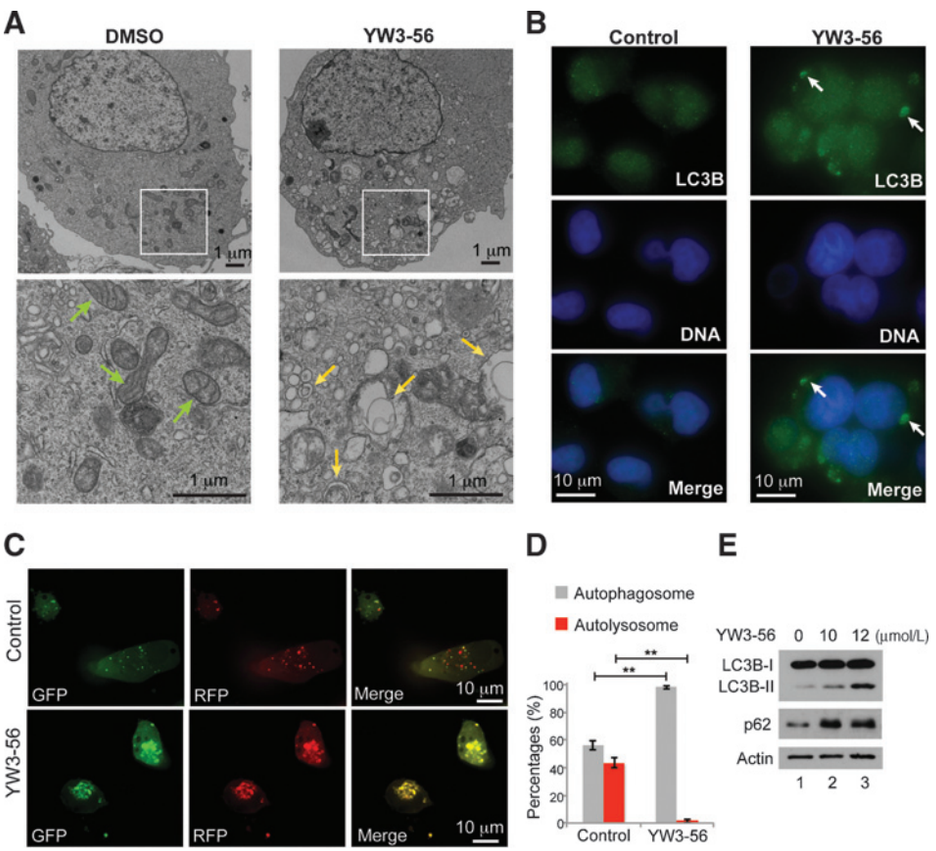

Figure 6.
YW3-56 induces cell death by affecting autophagy flux. A, TEM images of control MDA-MB-231 cells showing normal cellular structures with mitochondria denoted by green arrows. In contrast, YW3-56–treated MDA-MB-231 cells showed large numbers of autophagic vesicles denoted by yellow arrows. Note the disappearance of mitochondria. B, immunostaining of LC3B (green) in control and YW3-56–treated cells, noting the increased LC3B staining and LC3B speckles in YW3-56–treated cells. DNA (blue) was stained by Hoechst. C, YW3-56 inhibits autophagosome maturation to autolysosomes as measured by live cell imaging using the mCherry-GFP-LC3B reporter protein based on the quenching of the GFP signals by the acidic environment within autolysosomes. D, percentages of autophagosomes and autolysosomes identified in control and YW3-56–treated cells based on the GFP and RFP fluorescent signals. After YW3-56 treatment, the number of speckles with both RFP and GFP signals (representing autolysosomes) was increased from about 56% ($n = 19$) to about 98% ($n = 23$), **, $P < 0.002$. E, effect of YW3-56 on autophagy regulatory protein LC3B and p62/SQSTM1.

Published OnlineFirst January 22, 2015; DOI: 10.1158/1535-7163.MCT-14-1093-T

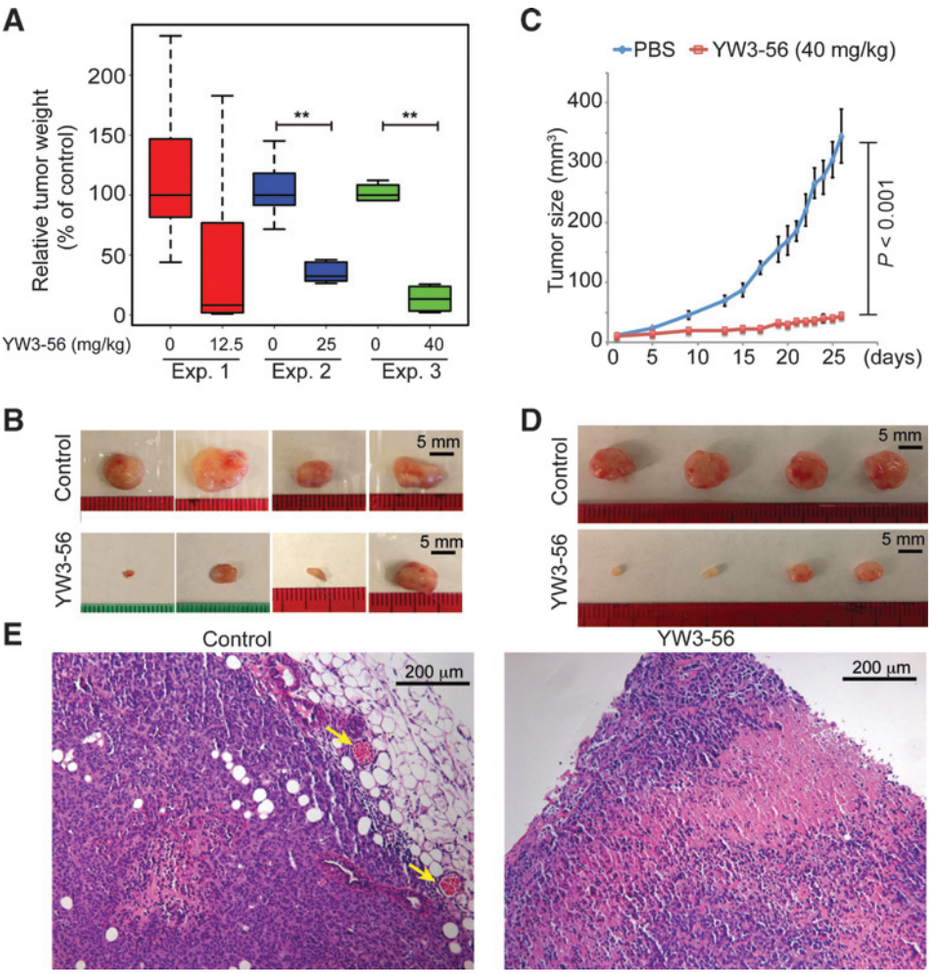

Figure 7.
Growth inhibition effects of YW3-56 on xenograft tumors of the triple-negative breast cancer 1833 cells. A, box plot showing the relative tumor weight (control tumors normalized to 100%, $n = 6$) obtained from three xenograft experiments with different dosage of YW3-56. **, $P < 0.002$. B, images of tumors in control and daily 12.5 mg/kg YW3-56 treatment groups. C, growth curves of tumors after treatment without or with 40 mg/kg YW3-56 once every 2 days. D, images of tumors without or with 40 mg/kg YW3-56 treatment once every 2 days. E, representative pathology hematoxylin and eosin (H&E) staining of the control and YW3-56–treated tumors. Yellow arrows denote blood vessels.

suggest that the autophagy flux was blocked after YW3-56 treatment.

YW3-56 inhibits the growth of MDA-MB-231–derived tumors in nude mice

To test whether YW3-56 is effective in inhibiting the growth of xenograft tumors derived from the triple-negative breast cancer cells, we used the 1833 cells that are derived from the parental MDA-MB-231 cells after bone metastasis (55). Three experiments with different dosage of YW3-56 were performed, and the percentage of tumor growth inhibition was tallied (Fig. 7A). At the 12.5 mg/kg dosage, a binary response to YW3-56 was observed: 2 tumors showed little response, whereas the other 4 tumors showed significant growth inhibition (Fig. 7B). The images of dissected tumors showed the size and morphology difference of these tumors (Fig. 7B). In tumors that showed growth inhibition (4L and 5L), an increase in the expression of YW3-56–inducible genes (e.g., SENS2 and DDIT4) was detected by qRT-PCR (Table 2). In contrast, in the tumor with no drug response (6L), these genes were largely unaltered (Table 2), suggesting an effective YW3-56 concentration did not achieve in the tumors without response.

When YW3-56 was used at 25 mg/kg body weight daily or 40 mg/kg body weight once every 2 days, significant tumor growth inhibition was detected (Fig. 7A). At the 40 mg/kg dosage, we found that all tumors ($n = 6$) grew much slower after drug treatment (Fig. 7C). The images of dissected tumors showed a decrease in tumor size after YW3-56 treatment (Fig. 7D). Analyses of gene expression in these xenograft tumors found an increase in

Table 2. Effects of YW3-56 on gene expression in xenograft tumors

Treatment	PBS	YW3-56 (12.5 mg/kg)			PBS	YW3-56 (40 mg/kg)	
Genes		4L	5L	6L		1R	11L
SESN2	1 ± 0.22	5.4	83.2	1.5	1 ± 0.08	22.1	5.3
DDIT4	1 ± 0.03	19.8	3.9	1.4	1 ± 0.22	1.4	2.2
GADD45	1 ± 0.08	5.0	5.1	0.7	1 ± 0.06	13.2	1.1
PUMA	1 ± 0.22	2.6	116.8	1.1	1 ± 0.11	23.9	5.1
DDIT3	1 ± 0.14	1.8	63.7	1.9	1 ± 0.23	24.2	2.1

the expression of YW3-56 inducible genes (Table 2). Pathologic analyses found less red blood cells and less fat tissues at the tumor surface after YW3-56 treatment (Fig. 7E), suggesting that YW3-56 affects multiple biologic aspects of tumor growth in mice.

Discussion

In summary, we identified ATF4 as an essential transcription factor mediating the expression of mTOR upstream regulatory genes DDIT4 and SESN2 after YW3-56 treatment. The ATF4–SESN2/DDIT4–mTOR signaling circuit offers a molecular link between YW3-56 and the mTORC1 signaling pathway. High-resolution mapping of ATF4- and CEBPB-binding sites using the ChIP-exo method revealed the gene networks and biologic pathways they regulate. YW3-56 induces the ER stress response and inhibits the autophagy flux in the triple-negative breast cancer cells. These cellular pathways synergize to induce cell growth inhibition and cell death. Finally, we showed that YW3-56 is effective in the inhibition of triple negative p53-mutant breast tumor growth in a xenograft model. Overall, YW3-56 offers a potential new therapeutic agent by altering gene expression in cancer cells.

Cancer cells explore the various survival mechanisms to cope with environmental stresses and become addictive to these pathways. Compound exacerbating the ER stress by inhibiting protein degradation (e.g., borezomib) is capable of pushing cancers over the cliff of cell death (60). Likewise, inhibitors of autophagy can inhibit cancer growth (19). In our work, YW3-56 perturbs multiple processes required for cancer growth, including the ER stress induction and autophagy inhibition. Given these pleiotropic effects, it is not surprising that YW3-56 inhibits the growth of tumor cells with diverse tissue origins and genetic background.

ATF4 is a basic leucine zipper (bZIP) type of transcription factor that can be induced by various stress conditions, including hypoxia, ER stress, and starvation (24, 25, 61, 62). The depletion of ATF4 significantly decreased YW3-56–induced SESN2 and DDIT4 expression at both protein and mRNA levels, whereas forced expression of ATF4 was sufficient for the SESN2 and DDIT4 expression increase, suggesting that ATF4 is both required and sufficient in mediating the expression of SESN2 and DDIT4 after YW3-56 treatment. During the process to prepare our work for publication, a report showed that protease inhibitor drugs nelfinavir and bortezomib induces SESN2 via ATF4 (63), raising an interesting possibility that SESN2 is a common effector linking ER stress drugs and the mTORC1 signaling pathway.

Disclosure of Potential Conflicts of Interest

B.F. Pugh is Founder/Co-Owner of Peconic, Inc. No potential conflicts of interest were disclosed by the other authors.

Authors' Contributions

Conception and design: S. Wang, B.F. Pugh, Y. Wang
Development of methodology: S. Wang, X.A. Chen, Y. Li, C. Thomas, B.F. Pugh
Acquisition of data (provided animals, acquired and managed patients, provided facilities, etc.): S. Wang, X.A. Chen, J. Hu, Y. Gu, B.F. Pugh, Y. Wang
Analysis and interpretation of data (e.g., statistical analysis, biostatistics, computational analysis): S. Wang, X.A. Chen, J. Hu, Y. Li, C. Thomas, B.F. Pugh, Y. Wang
Writing, review, and/or revision of the manuscript: S. Wang, X.A. Chen, C. Thomas, B.F. Pugh, Y. Wang
Administrative, technical, or material support (i.e., reporting or organizing data, constructing databases): S. Wang, K.Y. Chan-Salis, Y. Gu, Y. Wang
Study supervision: G. Chen, C. Thomas, Y. Wang
Other (provided material for the study and synthesized the compound YW3-56 for study): J.-k. Jiang

Acknowledgments

The authors thank Drs. Joan Massagué, Yibin Kang, and Andrea Mastro for cell lines and Drs. Terje Johansen and Tso-Pang Yao for reagents. They also thank laboratory members and members of the Center for Eukaryotic Gene Regulation for comments and helpful discussions. They thank the Penn State University Microscopy and Cytometry Facility and the Genomics Core Facility for technical help and thank Dr. Ying Gu from Penn State University for help with microscope imaging.

Grant Support

This work was supported by a NIH/NCI grant R01 CA136856 and a PBCC grant to Y. Wang.

The costs of publication of this article were defrayed in part by the payment of page charges. This article must therefore be hereby marked *advertisement* in accordance with 18 U.S.C. Section 1734 solely to indicate this fact.

Received January 5, 2015; accepted January 12, 2015; published OnlineFirst January 22, 2015.

References

1. Iwase S, Lan F, Bayliss P, de la Torre-Ubieta L, Huarte M, Qi HH, et al. The X-linked mental retardation gene SMCX/JARID1C defines a family of histone H3 lysine 4 demethylases. Cell 2007;128:1077–88.
2. Sandoval J, Esteller M. Cancer epigenomics: beyond genomics. Curr Opin Genet Dev 2012;22:50–5.
3. Shih AH, Abdel-Wahab O, Patel JP, Levine RL. The role of mutations in epigenetic regulators in myeloid malignancies. Nat Rev Cancer 2012;12:599–612.
4. Daigle SR, Olhava EJ, Therkelsen CA, Majer CR, Sneeringer CJ, Song J, et al. Selective killing of mixed lineage leukemia cells by a potent small-molecule DOT1L inhibitor. Cancer Cell 2011;20:53–65.
5. Delmore JE, Issa GC, Lemieux ME, Rahl PB, Shi J, Jacobs HM, et al. BET bromodomain inhibition as a therapeutic strategy to target c-Myc. Cell 2011;146:904–17.
6. Wang Y, Li P, Wang S, Hu J, Chen XA, Wu J, et al. Anticancer peptidylarginine deiminase (PAD) inhibitors regulate the autophagy flux and the mammalian target of rapamycin complex 1 activity. J Biol Chem 2012;287:25941–53.
7. Zuber J, Shi J, Wang E, Rappaport AR, Herrmann H, Sison EA, et al. RNAi screen identifies Brd4 as a therapeutic target in acute myeloid leukaemia. Nature 2011;478:524–8.
8. Vossenaar ER, Zendman AJ, van Venrooij WJ, Pruijn GJ. PAD, a growing family of citrullinating enzymes: genes, features and involvement in disease. Bioessays 2003;25:1106–18.
9. Wang S, Wang Y. Peptidylarginine deiminases in citrullination, gene regulation, health and pathogenesis. Biochim Biophys Acta 2013;1829:1126–35.
10. Cuthbert GL, Daujat S, Snowden AW, Erdjument-Bromage H, Hagiwara T, Yamada M, et al. Histone deimination antagonizes arginine methylation. Cell 2004;118:545–53.
11. Wang Y, Wysocka J, Sayegh J, Lee YH, Perlin JR, Leonelli L, et al. Human PAD4 regulates histone arginine methylation levels via demethylimination. Science 2004;306:279–83.
12. Li P, Wang D, Yao H, Doret P, Hao G, Shen Q, et al. Coordination of PAD4 and HDAC2 in the regulation of p53-target gene expression. Oncogene 2010;29:3153–62.
13. Li P, Yao H, Zhang Z, Li M, Luo Y, Thompson PR, et al. Regulation of p53 target gene expression by peptidylarginine deiminase 4. Mol Cell Biol 2008;28:4745–58.
14. Zhang X, Gamble MJ, Stadler S, Cherrington BD, Causey CP, Thompson PR, et al. Genome-wide analysis reveals PADI4 cooperates with Elk-1 to activate c-Fos expression in breast cancer cells. PLoS Genet 2011;7:e1002112.

15. Tanikawa C, Espinosa M, Suzuki A, Masuda K, Yamamoto K, Tsuchiya E, et al. Regulation of histone modification and chromatin structure by the p53-PADI4 pathway. Nat Commun 2012;3:676.
16. Leshner M, Wang S, Lewis C, Zheng H, Chen XA, Santy L, et al. PAD4 mediated histone hypercitrullination induces heterochromatin decondensation and chromatin unfolding to form neutrophil extracellular trap-like structures. Front Immunol 2012;3:307.
17. Sharma P, Azebi S, England P, Christensen T, Moller-Larsen A, Petersen T, et al. Citrullination of histone H3 interferes with HP1-mediated transcriptional repression. PLoS Genet 2012;8:e1002934.
18. Wellen KE, Thompson CB. Cellular metabolic stress: considering how cells respond to nutrient excess. Mol Cell 2010;40:323–32.
19. Yang S, Wang X, Contino G, Liesa M, Sahin E, Ying H, et al. Pancreatic cancers require autophagy for tumor growth. Genes Dev 2011;25:717–29.
20. Dang CV. Links between metabolism and cancer. Genes Dev 2012;26:877–90.
21. Vogelstein B, Lane D, Levine AJ. Surfing the p53 network. Nature 2000;408:307–10.
22. Vousden KH, Prives C. Blinded by the light: the growing complexity of p53. Cell 2009;137:413–31.
23. Kandoth C, McLellan MD, Vandin F, Ye K, Niu B, Lu C, et al. Mutational landscape and significance across 12 major cancer types. Nature 2013;502:333–9.
24. Ameri K, Harris AL. Activating transcription factor 4. Int J Biochem Cell Biol 2008;40:14–21.
25. Rzymski T, Milani M, Singleton DC, Harris AL. Role of ATF4 in regulation of autophagy and resistance to drugs and hypoxia. Cell Cycle 2009;8:3838–47.
26. Holz MS, Janning A, Renne C, Gatttenlohner S, Spieker T, Brauninger A. Induction of endoplasmic reticulum stress by sorafenib and activation of NF-kappaB by lestaurtinib as a novel resistance mechanism in Hodgkin lymphoma cell lines. Mol Cancer Ther 2013;12:173–83.
27. Hotamisligil GS. Endoplasmic reticulum stress and the inflammatory basis of metabolic disease. Cell 2010;140:900–17.
28. Harding HP, Zhang Y, Zeng H, Novoa I, Lu PD, Calfon M, et al. An integrated stress response regulates amino acid metabolism and resistance to oxidative stress. Mol Cell 2003;11:619–33.
29. Tabas I, Ron D. Integrating the mechanisms of apoptosis induced by endoplasmic reticulum stress. Nat Cell Biol 2011;13:184–90.
30. Walter P, Ron D. The unfolded protein response: from stress pathway to homeostatic regulation. Science 2011;334:1081–6.
31. Avivar-Valderas A, Salas E, Bobrovnikova-Marjon E, Diehl JA, Nagi C, Debnath J, et al. PERK integrates autophagy and oxidative stress responses to promote survival during extracellular matrix detachment. Mol Cell Biol 2011;31:3616–29.
32. Galehdar Z, Swan P, Fuerth B, Callaghan SM, Park DS, Cregan SP. Neuronal apoptosis induced by endoplasmic reticulum stress is regulated by ATF4-CHOP-mediated induction of the Bcl-2 homology 3-only member PUMA. J Neurosci 2010;30:16938–48.
33. Lin HK, Chen Z, Wang G, Nardella C, Lee SW, Chan CH, et al. Skp2 targeting suppresses tumorigenesis by Arf-p53-independent cellular senescence. Nature 2010;464:374–9.
34. Milani M, Rzymski T, Mellor HR, Pike L, Bottini A, Generali D, et al. The role of ATF4 stabilization and autophagy in resistance of breast cancer cells treated with Bortezomib. Cancer Res 2009;69:4415–23.
35. Mizushima N. Autophagy: process and function. Genes Dev 2007;21:2861–73.
36. Mizushima N, Levine B, Cuervo AM, Klionsky DJ. Autophagy fights disease through cellular self-digestion. Nature 2008;451:1069–75.
37. Bjorkoy G, Lamark T, Brech A, Outzen H, Perander M, Overvatn A, et al. p62/SQSTM1 forms protein aggregates degraded by autophagy and has a protective effect on huntingtin-induced cell death. J Cell Biol 2005;171:603–14.
38. Kroemer G, Marino G, Levine B. Autophagy and the integrated stress response. Mol Cell 2010;40:280–93.
39. Kon M, Kiffin R, Koga H, Chapochnick J, Macian F, Varticovski L, et al. Chaperone-mediated autophagy is required for tumor growth. Sci Transl Med 2011;3:109ra17.
40. Wang RC, Wei Y, An Z, Zou Z, Xiao G, Bhagat G, et al. Akt-mediated regulation of autophagy and tumorigenesis through Beclin 1 phosphorylation. Science 2012;338:956–9.
41. Amaravadi RK, Lippincott-Schwartz J, Yin XM, Weiss WA, Takebe N, Timmer W, et al. Principles and current strategies for targeting autophagy for cancer treatment. Clin Cancer Res 2011;17:654–66.
42. Leu JI, Pimkina J, Frank A, Murphy ME, George DL. A small molecule inhibitor of inducible heat shock protein 70. Mol Cell 2009;36:15–27.
43. Li P, Li M, Lindberg MR, Kennett MJ, Xiong N, Wang Y. PAD4 is essential for antibacterial innate immunity mediated by neutrophil extracellular traps. J Exp Med 2010;207:1853–62.
44. Rhee HS, Pugh BF. ChIP-exo method for identifying genomic location of DNA-binding proteins with near-single-nucleotide accuracy. Curr Protoc Mol Biol 2012;Chapter 21:Unit 21 4.
45. Rhee HS, Pugh BF. Comprehensive genome-wide protein-DNA interactions detected at single-nucleotide resolution. Cell 2011;147:1408–19.
46. Li H, Durbin R. Fast and accurate short read alignment with Burrows-Wheeler transform. Bioinformatics 2009;25:1754–60.
47. Albert I, Mavrich TN, Tomsho LP, Qi J, Zanton SJ, Schuster SC, et al. Translational and rotational settings of H2A.Z nucleosomes across the Saccharomyces cerevisiae genome. Nature 2007;446:572–6.
48. Albert I, Wachi S, Jiang C, Pugh BF. GeneTrack–a genomic data processing and visualization framework. Bioinformatics 2008;24:1305–6.
49. Bailey TL, Boden M, Buske FA, Frith M, Grant CE, Clementi L, et al. MEME SUITE: tools for motif discovery and searching. Nucleic Acids Res 2009;37:W202–8.
50. Machanick P, Bailey TL. MEME-ChIP: motif analysis of large DNA datasets. Bioinformatics 2011;27:1696–7.
51. Grant CE, Bailey TL, Noble WS. FIMO: scanning for occurrences of a given motif. Bioinformatics 2011;27:1017–8.
52. Huang da W, Sherman BT, Lempicki RA. Systematic and integrative analysis of large gene lists using DAVID bioinformatics resources. Nat Protoc 2009;4:44–57.
53. Emig D, Salomonis N, Baumbach J, Lengauer T, Conklin BR, Albrecht M. AltAnalyze and DomainGraph: analyzing and visualizing exon expression data. Nucleic Acids Res 2010;38:W755–62.
54. Subramanian A, Tamayo P, Mootha VK, Mukherjee S, Ebert BL, Gillette MA, et al. Gene set enrichment analysis: a knowledge-based approach for interpreting genome-wide expression profiles. Proc Natl Acad Sci U S A 2005;102:15545–50.
55. Kang Y, Siegel PM, Shu W, Drobnjak M, Kakonen SM, Cordon-Cardo C, et al. A multigenic program mediating breast cancer metastasis to bone. Cancer Cell 2003;3:537–49.
56. Budanov AV, Karin M. p53 target genes sestrin1 and sestrin2 connect genotoxic stress and mTOR signaling. Cell 2008;134:451–60.
57. Lee JH, Budanov AV, Talukdar S, Park EJ, Park HL, Park HW, et al. Maintenance of metabolic homeostasis by Sestrin2 and Sestrin3. Cell Metab 2012;16:311–21.
58. Johnson PF. Molecular stop signs: regulation of cell-cycle arrest by C/EBP transcription factors. J Cell Sci 2005;118:2545–55.
59. Podust LM, Krezel AM, Kim Y. Crystal structure of the CCAAT box/enhancer-binding protein beta activating transcription factor-4 basic leucine zipper heterodimer in the absence of DNA. J Biol Chem 2001;276:505–13.
60. Fanucchi MP, Fossella FV, Belt R, Natale R, Fidias P, Carbone DP, et al. Randomized phase II study of bortezomib alone and bortezomib in combination with docetaxel in previously treated advanced non-small-cell lung cancer. J Clin Oncol 2006;24:5025–33.
61. Whitney ML, Jefferson LS, Kimball SR. ATF4 is necessary and sufficient for ER stress-induced upregulation of REDD1 expression. Biochem Biophys Res Commun 2009;379:451–5.
62. Brugarolas J, Lei K, Hurley RL, Manning BD, Reiling JH, Hafen E, et al. Regulation of mTOR function in response to hypoxia by REDD1 and the TSC1/TSC2 tumor suppressor complex. Genes Dev 2004;18:2893–904.
63. Bruning A, Rahmeh M, Friese K. Nelfinavir and bortezomib inhibit mTOR activity via ATF4-mediated sestrin-2 regulation. Mol Oncol 2013;7:1012–8.

Published OnlineFirst January 22, 2015; DOI: 10.1158/1535-7163.MCT-14-1093-T

Molecular Cancer Therapeutics

ATF4 Gene Network Mediates Cellular Response to the Anticancer PAD Inhibitor YW3-56 in Triple-Negative Breast Cancer Cells

Shu Wang, Xiangyun Amy Chen, Jing Hu, et al.

Mol Cancer Ther 2015;14:877-888. Published OnlineFirst January 22, 2015.